Metallaborane Chemistry. Part 11.[1] Lower Rotational Barriers in Seven-vertex than in Twelve-vertex Carbaplatinaboranes: Synthesis, and Molecular and Crystal Structures of [*closo*-1,1-$(Et_3P)_2$-2,3-Me_2-1,2,3-$PtC_2B_4H_4$] and [*closo*-1,1-$(Et_3P)_2$-1,2,4-$PtC_2B_4H_6$] *

By **Geoffrey K. Barker, Michael Green,** and **F. Gordon A. Stone,** Department of Inorganic Chemistry, The University, Bristol BS8 1TS
Alan J. Welch, Department of Chemistry, The City University, London EC1V OHB

Sealed-tube pyrolysis of [*nido*-$\mu_{4,5}$-{*trans*-$(Et_3P)_2Pt(H)$}-$\mu_{5,6}$-H-2,3-Me_2-2,3-$C_2B_4H_4$] affords the *closo*-carbametallaborane [1,1-$(Et_3P)_2$-2,3-Me_2-1,2,3-$PtC_2B_4H_4$], structurally characterised by *X*-ray diffraction. Crystals are monoclinic, space group $P2_1/a$, $Z = 4$, in a unit cell with lattice parameters $a = 15.691(6)$, $b = 10.118(6)$, $c = 15.949(6)$ Å, and $\beta = 115.76(3)°$. Using 7 437 data collected at 215 K on a four-circle diffractometer, refinement converged at R 0.067. The molecule has a highly distorted pentagonal-bipyramidal cage with a novel (C_{2v}) conformation of the $Pt(PEt_3)_2$ fragment. In contrast, pyrolysis of [*nido*-$\mu_{4,5}$-{*trans*-$(Et_3P)_2Pt(H)$}-$\mu_{5,6}$-H-2,3-$C_2B_4H_6$] proceeds with separation of the cage carbon atoms, affording [*closo*-1,1-$(Et_3P)_2$-1,2,4-$PtC_2B_4H_6$], which may alternatively be prepared directly from 1,6-$C_2B_4H_6$ or 5-Me_3N-2,4-$C_2B_4H_6$. A crystallographic study of this *closo*-carbametallaborane confirms the cage carbon positions. Crystals are monoclinic, space group $P2_1/n$, with eight molecules in a unit cell of dimensions $a = 16.045(7)$, $b = 17.354(5)$, $c = 16.918(6)$ Å, and $\beta = 117.11(3)°$. Refinement converged to R 0.043 for 8 275 data recorded at 215 K. The two crystallographically independent molecules in the asymmetric unit both have pentagonal-bipyramidal cages, but are related as rotational conformers about the metal–cage axis. Comparison of the molecular parameters of the three seven-vertex cages thus studied with those of analogous 12-vertex (icosahedral) systems suggests that the barrier to rotation of a metal fragment, about the axis linking it to the cage, should be less in the former case, and this has been verified by variable-temperature n.m.r. studies.

In the preceding paper [1] of this series we described the synthesis and, in one case, the solid-state molecular structure of compounds of the type [*nido*-$\mu_{4,5}$-{*trans*-$(R'_3P)_2Pt(H)$}-$\mu_{5,6}$-H-2,3-R_2-2,3-$C_2B_4H_4$] (1a, R = H, R' = Et; 1b, R = Me, R' = Et) and [*nido*-$\mu_{3,4}$-H-$\mu_{4,5}$-{*trans*-$(R'_3P)_2Pt(H)$}-$\mu_{5,6}$-H-2-CB_5H_6] (2), formed by the formal oxidative insertion of a $[Pt(PR'_3)_2]$ fragment into a B(μ-H)B bond of the *nido*-carbaboranes 2,3-R_2-2,3-$C_2B_4H_6$ and 2-CB_5H_9, respectively. This work represented an extension of our previous studies [2-7] on the synthetic and structural aspects of carbametallaboranes formed by the direct insertion of a highly nucleophilic $[Pt(PR_3)_2]$ or $[Pd(CNBu^t)_2]$ fragment into *closo*-carbaboranes, a technique affording, amongst others, the 12-vertex icosahedral species [1,1-$(PhMe_2P)_2$-2,4-Me_2-1,2,4-$PtC_2B_9H_9$] (3),[2,3] [2,2-$(Bu^tNC)_2$-1-Me_3N-2,1-$PdCB_{10}H_{10}$] (4),[5] and [3,3-$(Et_3P)_2$-3,2,1-$PtC_2B_9H_{11}$] (5).[8]

In compounds (3)—(5) the orientations and ' slipping ' distortions of the ML_2 groups (both defined with respect to the polyhedron) were found to be highly selective. Subsequent molecular-orbital (m.o.) calculations by Mingos *et al.*[8,9] have demonstrated that the number and positions of carbon atoms in the metalla-bonded polyhedral face are largely responsible for the observed features.

Herein we describe the synthesis, and the molecular and crystal structures, of the compounds [*closo*-1,1-$(Et_3P)_2$-2,3-Me_2-1,2,3-$PtC_2B_4H_4$] (6), and [*closo*-1,1-$(Et_3P)_2$-1,2,4-$PtC_2B_4H_6$] (7a); two isomers of the seven-vertex carbaplatinaborane $[Pt(PEt_3)_2(R_2C_2B_4H_4)]$ whose polyhedral skeletons differ only in respect of the positions of the cage carbon atoms. *closo*-Seven-atom carbametallaboranes are expected to be structurally based on the pentagonal bipyramid, and in all previous, crystallographically authenticated, examples [10-15] the metal atom is found, without exception, to occupy an apical † site in the polyhedron. Thus, seven- and 12-atom carbametallaboranes are directly comparable since in both the pentagonal bipyramid and the icosahedron, a five-connected (with respect to the cage) metal atom is bound to a pentagonal-polyhedral face that is planar to a first approximation. However, the possibility of subtle differences arises, since the pentagonal rings of seven-atom species are generally smaller than those of chemically similar icosahedra and, further, the elevation angles of substituents terminally bound to these rings are quite different. The present studies were initiated to determine the possible consequences of these differences in carbaplatinaboranes. Some aspects of this work have previously been communicated.[16]

RESULTS AND DISCUSSION

The species [*nido*-$\mu_{4,5}$-{*trans*-$(Et_3P)_2Pt(H)$}-$\mu_{5,6}$-H-2,3-$C_2B_4H_6$] (1a) and [*nido*-$\mu_{4,5}$-{*trans*-$(Et_3P)_2Pt(H)$}-$\mu_{5,6}$-H-2,3-Me_2-2,3-$C_2B_4H_4$] (1b) lose a molecule of hydrogen on heating (100 °C, hexane solution) in a sealed tube to form, respectively, the yellow crystalline complexes (7a) and (6), which were identified by elemental analysis, i.r., mass, and n.m.r. spectroscopy as *closo*-carbaplatinabo-

* 2,3-Dimethyl-1,1-bis(triethylphosphine)-2,3-dicarba-1-platina-*closo*-heptaborane and 1,1-bis(triethylphosphine)-2,4-dicarba-1-platina-*closo*-heptaborane, respectively.

† In the pentagonal bipyramid ' apical ' vertices are five-connected whilst ' equatorial ' vertices are four-connected with respect to the polyhedron.

ranes with molecular formula $[Pt(PEt_3)_2(R_2C_2B_4H_4)]$ (R = H or Me). Although there is insufficient evidence available to establish firmly the details of this fragmentation reaction, it is likely that the penultimate step involves a species where both of the hydrogen atoms which are to form H_2 are bonded to the platinum in a relative *cis* configuration. Such a species could be formed by loss of the acidic 5,6-B(μ-H)B proton followed by protonation [$Pt^{II} \rightarrow Pt^{IV}$] of the platinum.

Comparison of the ^{11}B n.m.r. shifts for (6) and (7a) clearly suggests the existence of two isomeric types differing in the relative positions of the cage carbon atoms. The simplest explanation for this difference is that a thermally induced polyhedral rearrangement occurs in one case only. However, the fact (see later) that this occurs more readily with the system which does *not* carry substituents on the cage carbon atoms is

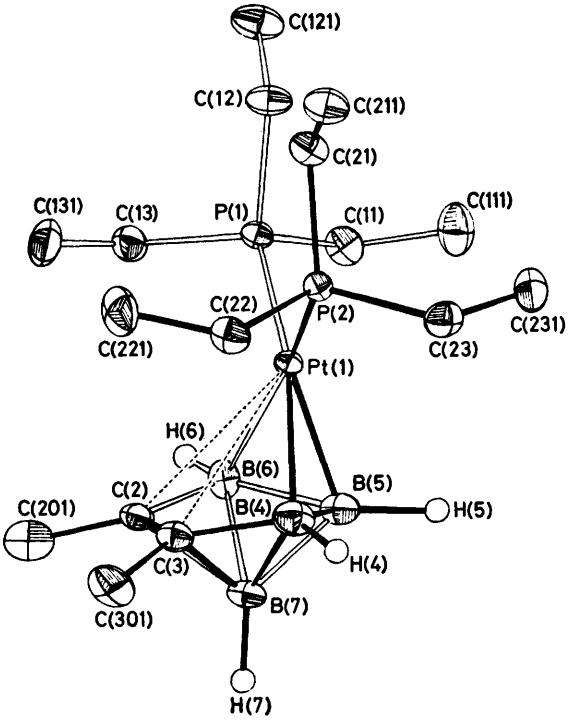

FIGURE 1 Perspective view of a molecule of compound (6). Thermal ellipsoids are drawn enclosing 50% electron probability, except for the cage hydrogen atoms which have an artificial radius of 0.1 Å. Hydrogens of the ethyl groups are not shown for clarity

surprising. The *closo*-carbaplatinaborane (7a) with non-adjacent cage carbon atoms was also formed on reaction (60 °C) of *closo*-1,6-$C_2B_4H_6$ with $[Pt_2(\mu\text{-cod})(PEt_3)_4]$ (cod = cyclo-octa-1,5-diene), and extension of the reaction to *closo*-1,6-Me_2-1,6-$C_2B_4H_4$ afforded the dimethyl analogue (7b) as a yellow crystalline material. It is interesting that (7a) was also formed in moderate yield by the reaction at room temperature of the adduct 5-Me_3N-2,4-$C_2B_4H_6$, obtained by addition of Me_3N to *closo*-1,6-$C_2B_4H_6$, with $[Pt_2(\mu\text{-cod})(PEt_3)_4]$.

* Phosphorus atoms are numbered differently from that communicated in ref. 16.

In order to establish unambiguously the structures of these compounds, and to determine molecular parameters to be set against those of the corresponding icosahedral structures, single-crystal *X*-ray diffraction experiments were carried out with suitable crystals of (6) and (7a).

Figure 1 presents a perspective view of a single molecule of (6) and demonstrates the atomic numbering scheme

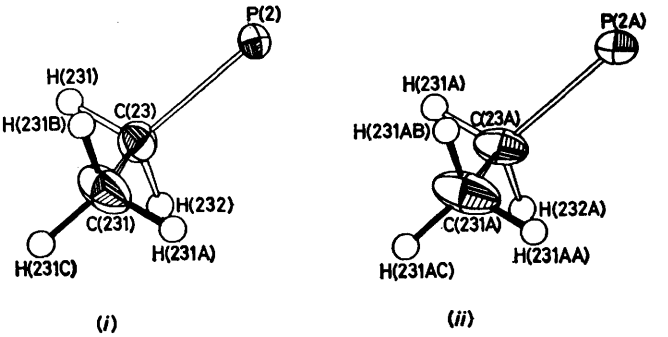

FIGURE 2 Typical ethyl hydrogen atom numbering systems used in, (*i*) compound (6), and (*ii*) compound (7a)

adopted.* As detailed in the experimental section, cage hydrogen atoms were located and positionally refined, whilst those of the ethyl groups were idealized. Figure 2(*i*) presents the ethyl hydrogen numbering scheme used for each group. The hydrogen atoms of the cage methyl groups were not found.

Interatomic distances, uncorrected for thermal effects, are listed in Table 1 and selected angles are given in Table 2 (those involving cage hydrogens appear in Appendix A).†

TABLE 1

Interatomic distances (Å) for the compound [*closo*-1,1-$(Et_3P)_2$-2,3-Me_2-1,2,3-$PtC_2B_4H_4$] (6)

Pt(1) · · · C(2)	2.858(7) *	C(3)–C(301)	1.496(11)
Pt(1) · · · C(3)	2.851(6)	B(4)–H(4)	1.09(16)
Pt(1)–B(4)	2.257(8)	B(5)–H(5)	1.25(20)
Pt(1)–B(5)	2.129(10)	B(6)–H(6)	1.13(16)
Pt(1)–B(6)	2.244(8)	B(7)–H(7)	1.15(15)
C(2)–C(3)	1.427(10)	P(1)–C(11)	1.830(9)
C(2)–B(7)	1.764(13)	C(11)–C(111)	1.513(15)
C(2)–B(6)	1.581(11)	P(1)–C(12)	1.834(8)
C(3)–B(4)	1.575(14)	C(12)–C(121)	1.527(10)
C(3)–B(7)	1.777(14)	P(1)–C(13)	1.834(9)
B(4)–B(5)	1.739(14)	C(13)–C(131)	1.506(16)
B(4)–B(7)	1.824(13)	P(2)–C(21)	1.821(7)
B(5)–B(6)	1.732(13)	C(21)–C(211)	1.521(12)
B(5)–B(7)	1.664(12)	P(2)–C(22)	1.824(8)
B(6)–B(7)	1.828(10)	C(22)–C(221)	1.511(17)
Pt(1)–P(1)	2.273 7(16)	P(2)–C(23)	1.829(9)
Pt(1)–P(2)	2.285 4(21)	C(23)–C(231)	1.527(15)
C(2)–C(201)	1.508(13)		

* Estimated standard deviations in parentheses throughout this paper.

The analysis clearly establishes that, in compound (6), the cage carbon atoms are adjacent, *i.e.* thermolysis of (1b) proceeds *via* the elimination of H_2 and cage closure *but without carbon atom separation*. The overall geometry of the cage is that of a highly distorted pentagonal

†Appendices may be recovered from Supplementary Publication No. SUP 22754 (71 pp.). For details see Notices to Authors No. 7, *J.C.S. Dalton*, 1979, Index issue.

bipyramid in which atoms Pt(1) and B(7) are in apical sites. Although not a space group requirement, an effective mirror plane through atoms Pt(1), B(5), and B(7) bisects the polyhedron and, except for parameters involving the relatively uncertainly positioned cage hydrogen atoms, this mirror symmetry is valid to within two standard deviations for all deltahedral dimensions.

In common with all structural studies of metalla- and carbametalla-boranes, the polyhedron suffers major deformation from an idealized geometry simply because of the presence of the metal atom and to a lesser extent the carbon atoms. However, in (6) there are clearly additional polyhedral distortions to those expected, and these may be summarised as (i) a lateral shift or ' slip ' of the $[Pt(PEt_3)_2]$ moiety across the C_2B_3 polyhedral face towards B(5), and (ii) a buckling of that face.

In terms of the nature of the polyhedral face to which the metal fragment is attached, compound (6) is to be compared with the icosahedral species [3,3-$(Et_3P)_2$-3,2,1-$PtC_2B_9H_{11}$] (5), which we have previously studied.[8] In the latter, it was found that the PtP_2 unit adopted a perpendicular ($\perp$) orientation * with respect to the approximate cage mirror plane, and suffered a substantial, positive slip distortion (0.42 Å) across the metalla-bonded face (*i.e.* movement towards the unique boron atom 8). In addition, the C_2B_3 face of (5) was found to be substantially non-planar. Although we subsequently show (see below) that this non-planarity is more correctly described in terms of a skew ring conformation, it has previously proven more convenient to calculate the acute folding angle [*ca.* 9° in (5)] between the B_3 plane and best (least-squares) plane through the BCCB sequence as though the deformation were of the envelope type. The orientation, slip, and ' fold ' of (5) have successfully been rationalised as part of a general frontier-orbital analysis in which all three modes of substitution (two adjacent, two separate, and one single carbon atom) into the open face of a *nido*-icosahedral B_{11} fragment were considered.[8,9]

In Figure 3 we view the central portion of (6) along the bisector of the angle P(1)–Pt(1)–P(2). This projection, taken with the calculated dihedral angle between the PtP_2 plane and idealised cage mirror plane of 82.0° (Table 3), establishes that the PtP_2 orientation in (6) is also perpendicular. Compound (6) further resembles its icosahedral analogue (5) in that it, too, suffers a large, positive slipping distortion, as previously noted. Although it is not possible to estimate the magnitude of the slipping parameter in a seven-vertex polyhedron (due to the absence of a suitable reference plane) we believe it to be substantially greater in (6) than (5) for the following three reasons. (i) Pt–C distances are considerably longer in (6) than in (5) (mean values are 2.855 and 2.572 Å respectively). In previous studies of carbaplatinaboranes a Pt–C separation of 2.83 Å has nominally been taken [6a] as ' non-bonding ', and certainly

TABLE 2

Selected interbond angles (°) for compound (6)

(*a*) Deltahedral

C(2) · · · Pt(1) · · · C(3)	28.96(19)	Pt(1)–B(5)–B(6)	70.2(5)
C(3) · · · Pt(1)–B(4)	33.4(3)	B(6)–B(5)–B(7)	65.1(5)
B(4)–Pt(1)–B(5)	46.6(4)	B(7)–B(5)–B(4)	64.8(5)
B(5)–Pt(1)–B(6)	46.6(4)	B(4)–B(5)–Pt(1)	70.6(5)
B(6)–Pt(1) · · · C(2)	33.4(3)		
		Pt(1)–B(6)–C(2)	95.1(5)
Pt(1) · · · C(2)–C(3)	75.3(4)	C(2)–B(6)–B(7)	61.8(5)
C(3)–C(2)–B(7)	66.7(6)	B(7)–B(6)–B(5)	55.6(5)
B(7)–C(2)–B(6)	66.0(5)	B(5)–B(6)–Pt(1)	63.2(4)
B(6)–C(2) · · · Pt(1)	51.4(3)		
		C(2)–B(7)–C(3)	47.5(4)
Pt(1) · · · C(3)–B(4)	52.1(3)	C(3)–B(7)–B(4)	51.8(5)
B(4)–C(3)–B(7)	65.6(6)	B(4)–B(7)–B(5)	59.6(5)
B(7)–C(3)–C(2)	65.7(6)	B(5)–B(7)–B(6)	59.3(5)
C(2)–C(3) · · · Pt(1)	75.8(3)	B(6)–B(7)–C(2)	52.2(4)
Pt(1)–B(4)–B(5)	62.8(4)		
B(5)–B(4)–B(7)	55.6(5)		
B(7)–B(4)–C(3)	62.6(6)		
C(3)–B(4)–Pt(1)	94.5(5)		

(*b*) Polyhedral

P(1)–Pt(1)–P(2)	105.75(6)	C(201)–C(2) · · · Pt(1)	147.2(5)
P(1)–Pt(1) · · · C(2)	107.33(14)	C(201)–C(2)–C(3)	122.5(7)
P(1)–Pt(1) · · · C(3)	134.07(16)	C(201)–C(2)–B(7)	130.3(6)
P(1)–Pt(1)–B(4)	162.26(22)	C(201)–C(2)–B(6)	125.2(6)
P(1)–Pt(1)–B(5)	121.43(22)		
		C(301)–C(3) · · · Pt(1)	148.5(6)
P(1)–Pt(1)–B(6)	91.53(19)		
		C(301)–C(3)–B(4)	124.8(7)
P(2)–Pt(1) · · · C(2)	124.38(16)		
		C(301)–C(3)–B(7)	128.9(6)
P(2)–Pt(1) · · · C(3)	99.91(16)		
		C(301)–C(3)–C(2)	122.4(8)
P(2)–Pt(1)–B(4)	90.93(21)		
P(2)–Pt(1)–B(5)	128.12(23)		
P(2)–Pt(1)–B(6)	156.98(19)		

(*c*) Phosphine ligands

Pt(1)–P(1)–C(11)	109.7(3)	Pt(1)–P(2)–C(21)	122.3(2)
Pt(1)–P(1)–C(12)	122.4(2)	Pt(1)–P(2)–C(22)	110.6(3)
Pt(1)–P(1)–C(13)	112.7(2)	Pt(1)–P(2)–C(23)	111.8(3)
C(11)–P(1)–C(12)	102.9(4)	C(21)–P(2)–C(22)	102.9(4)
C(11)–P(1)–C(13)	103.7(4)	C(21)–P(2)–C(23)	104.4(4)
C(12)–P(1)–C(13)	103.5(4)	C(22)–P(2)–C(23)	102.8(4)
P(1)–C(11)–C(111)	113.4(6)	P(2)–C(21)–C(211)	118.1(5)
P(1)–C(12)–C(121)	116.8(6)	P(2)–C(22)–C(221)	112.9(5)
P(1)–C(13)–C(131)	113.1(7)	P(2)–C(23)–C(231)	112.7(6)

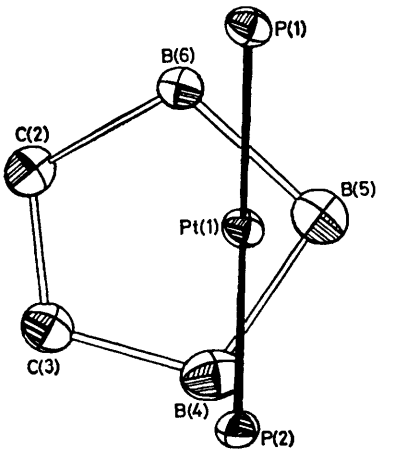

FIGURE 3 View along the bisector of the P–Pt–P angle of (6) to demonstrate the perpendicular orientation of the PtP_2 plane relative to that of the cage mirror. Metal–cage links are not shown for clarity

* See ref. 8 for definition of parallel and perpendicular orientations and slipping and folding distortions.

in the present case 2.85 Å must represent little, if any, significant interaction. Thus we show these links as only dashed lines in Figures 1 and 4, the latter reproducing the crystal packing in *b* axis projection.

TABLE 3

Least-squares molecular planes * for compound (6)

Each plane is defined by the equation $Px + Qy + Rz = S$, where x, y, and z are the atomic co-ordinates (Table 11). Individual atomic deviations (Å) are given in square brackets

	P	*Q*	*R*	*S*
Plane A: B(6)C(2)C(3)B(4)				
	13.264	−5.054	−3.135	0.294
[B(6) −0.004, C(2) 0.008, C(3) −0.008, B(4) 0.004, B(5) 0.419, Pt(1) −1.683, H(6) −0.124, C(201) 0.176, C(301) 0.187, H(4) 0.287]				
Plane B: B(4)B(5)B(6)				
	10.130	−5.912	2.588	1.555
[Pt(1) −1.833, C(2) 0.545, C(3) 0.524, H(4) 0.205, H(5) −0.110, H(6) −0.065]				
Plane C: Pt(1)P(1)P(2)				
	−8.964	−3.381	14.728	2.621
[B(4) 0.241, B(5) −0.695, B(6) 0.595]				
Plane D: Pt(1)B(5)B(7), *i.e.* idealised cage mirror plane				
	5.852	8.159	4.008	2.584

Dihedral angles (°): A–B 21.4 B–C 80.0 A–C 78.8 C–D 82.0

*All atoms have unit weight.

(ii) Pt–B distances are all shorter in (6) than in (5), with the greatest difference involving that boron atom [B(5) of the present compound] located on the slipping plane. Although one might initially imagine that an apical–equatorial link in a pentagonal bipyramid would anyway be somewhat shorter than a chemically similar link in an icosahedron (because of the lower cage connectivity number of equatorial atoms in the former) we will subsequently demonstrate that this is not, in fact, the case.

(iii) The folding of the metalla-bonded pentagonal face of (6), which may properly be described as of envelope conformation (see later), is in the same sense as that we have taken for (5) but considerably greater in magnitude (21.4° *vs.* 9.1°), and the folding and slipping distortions in molecules of this type have previously been shown [8] to be intimately related.

TABLE 4

Average B–B, B–C, and C–C distances (Å) in *closo*-carbametallaboranes structurally based on the icosahedron and pentagonal bipyramid [a]

Linkage	Average distance
(*a*) Icosahedron	
B–B	1.772
B–C	1.712
C–C	1.613
(*b*) Pentagonal bipyramid [b,c,d]	
$B_{eq.}$–$B_{eq.}$	1.712
$B_{ax.}$–$B_{eq.}$	1.774
$B_{eq.}$–C	1.568
$B_{ax.}$–C	1.743
C–C	1.461

[a] Adapted from ref. 25. [b] Subscripts describe vertices as equatorial or axial. [c] Data from compounds (6) and (7a) not included. [d] C atoms occur exclusively in equatorial sites.

A qualitative argument explaining these features is postponed until the structure of compound (7a) has been described below.

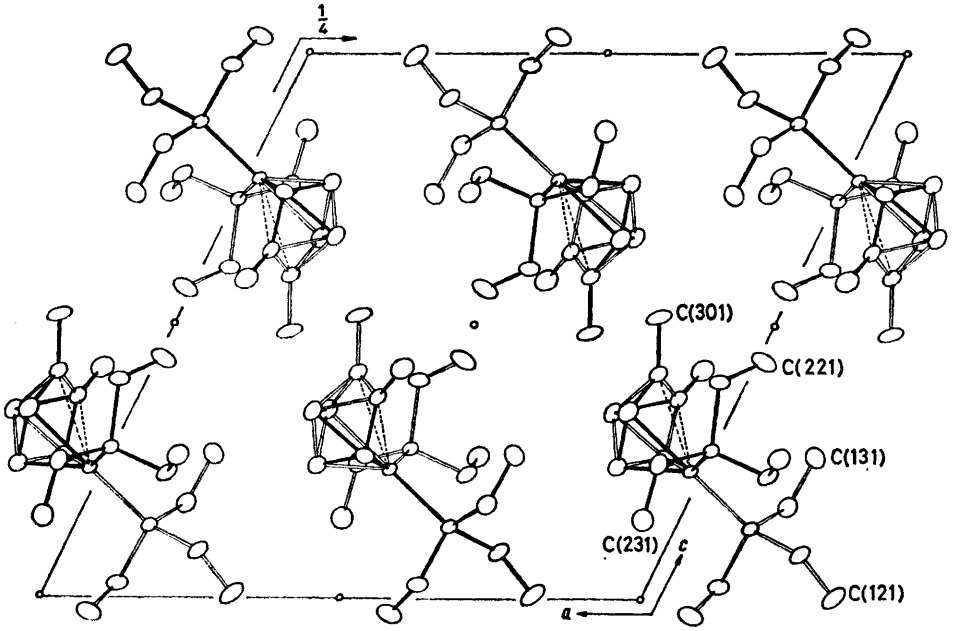

FIGURE 4 The molecular packing of (6) viewed along the *b* axis. No hydrogen atoms, and only the minimum symmetry elements to define the array, are shown for clarity

Previously, the crystal structures of only six carbametallaboranes with *closo*-pentagonal-bipyramidal architectures have been described [10–15] and, in the second part of Table 4, the mean B–B, B–C, and C–C internuclear distances there found are presented. The overall agreement between these figures and those found in

(6) is generally good, but there are two features worthy of comment. Firstly, C(2)–C(3) [1.427(10) Å] is the shortest such bond being *ca.* 0.03 Å less than the previous mean. Carbon–carbon bond shortening has already been recognised [8] as being associated with a positive slipping distortion in the analogous 12-atom family, and thus adds further evidence for a similar phenomenon here. Secondly, although $\langle B_{ax.}-B_{eq.}\rangle$ in (6), 1.772 Å, is identical to the established mean value, a more illuminating comparison is furnished by considering B(5)–B(7) with the pair B(4)–B(7) and B(6)–B(7) separately in *closo*-1-metalla-2,3-dicarbaheptaboranes. In (6) the former is shorter by *ca.* 0.16 Å, whereas in three previous studies [10,13,14] the same difference is only *ca.* 0.03—0.05 Å. This feature is clearly associated with the severe folding of the C_2B_3 pentagonal face of (6) already discussed.

The two cage methyl carbon atoms, which lie slightly (*ca.* 0.18 Å) out of the best (least-squares) plane through atoms B(6), C(2), C(3), and B(4) to the side of the metal atom, are at an average distance of 1.502 Å from their

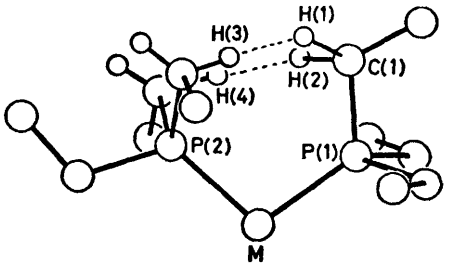

(*i*)

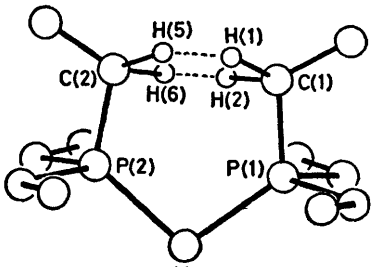

(*ii*)

FIGURE 5 Stereochemistries of *cis*-$M(PEt_3)_2$ fragments; (*i*) is more commonly observed and occurs in both molecules of (7a), whilst (*ii*) is seen for the first time in (6). H · · · H repulsive contacts are shown as dashed lines

bonded carbon atoms, which is quite normal for molecules of this type.[11,12,14] The two Pt–P bond lengths determined are statistically different at a confidence level greater than 99%, but almost certainly this merely reflects their low σ's since the chemical environments of the two PEt_3 functions are clearly equivalent.

To our knowledge the particular internal conformation displayed by the $M(PEt_3)_2$ moiety of (6) has not been previously observed. Most crystallographically studied examples of *cis*-$M(PEt_3)_2$ fragments [6,8,17-19] reveal the stereochemistry we have previously described [8] in the case of compound (5), in which the two halves of the fragment can be effectively superimposed by a rotation in the MP_2 plane, through the angle P–M–P. A consequence of this arrangement [drawn schematically in Figure 5(*i*)] appears to be the development of two repulsive interactions, H(1) · · · H(3) and H(2) · · · H(4), which, with one anomalous exception,[19] open up the M–P(1)–C(1) angle to *ca.* 120—122°, making it the largest such angle in the molecule.

In (6) the $Pt(PEt_3)_2$ fragment possesses effective C_{2v} symmetry, as shown in Figure 5(*ii*).* Again this leads to two repulsive contacts, H(1) · · · H(5) and H(2) · · · H(6), but this time the destabilising effect is accommodated by a widening of *two* angles, M–P(1)–C(1) and M–P(2)–C(2). In (6) these angles are Pt(1)–P(1)–C(12), 122.4(2)°, and Pt(1)–P(2)–C(21), 122.3(2)°, *cf.* 109.7(3)—112.7(2)° for the other four. In view of the fact that the P–M–P angle [105.76(6)°] in (6) is the widest of its type to have been observed, it is likely that this second stereochemistry is somewhat less favourable than the former. A more detailed assessment of the relative space-filling requirements of these and a third known conformation (of C_2 symmetry [20]) in *cis*-$M(PEt_3)_2$ fragments will be presented elsewhere.[21]

TABLE 5

Short H · · · H and H · · · Me contacts [a] (Å) in the crystal structure of [*closo*-1,1-$(Et_3P)_2$-2,3-Me_2-1,2,3-$PtC_2B_4H_4$], (6)

Atom A [b]	Atom B	Position B	Contact
(*a*) Intramolecular			
H(121)	H(212)	*x*, *y*, *z*	2.37
H(122)	H(211)	*x*, *y*, *z*	2.27
H(221)	C(301)	*x*, *y*, *z*	3.17
(*b*) Intermolecular			
H(5)	H(121)	$\frac{1}{2}+x$, $\frac{1}{2}-y$, *z*	2.22
H(211)	H(121A)	$-(\frac{1}{2}+x)$, $\frac{1}{2}-y$, $-z$	2.34
H(222)	H(221C)	$-x$, $1-y$, $1-z$	2.37
H(221C)	C(201)	$-x$, $-y$, $1-z$	3.15

[a] Van der Waal's radii taken as, H 1.20 Å, Me 2.00 Å. [b] Atom A is at co-ordinates *x*, *y*, *z*.

Table 5 gives intra- and inter-molecular contacts shorter than the appropriate van der Waals sum. The first two intramolecular interactions correspond to H(1) · · · H(5) and H(2) · · · H(6) of Figure 5(*ii*), but at 2.27 and 2.37 Å they are clearly no longer severe, suggesting sufficient flexibility in the $Pt(PEt_3)_2$ fragment of (6) to have effectively nullified these contacts *via* the deformations described.

The results of the structural investigation of compound (7a) reveal two crystallographically independent molecules, A and B, in the asymmetric fraction of the unit cell. In Figure 6 one molecule of each is projected onto its own PtP_2 plane in directions that reflect the common stereochemistry of each $Pt(PEt_3)_2$ moiety. The atom

* Figures 5(*i*) and (*ii*) are most simply inter-related by a 180° rotation of the [$Et_3P(2)$] group about the axis P(2)–M.

numbering in the phosphine ligands is in accord with this similarity, and the cage atoms are numbered cyclically in the usual fashion. For all non-hydrogen atoms the final letter denotes the molecule to which it belongs. Cage hydrogens carry the same number as their bonded boron or carbon atom, whilst the ethyl-H system [as with compound (6) these were set in idealised positions in the crystallographic analysis] is illustrated for one branch in Figure 2(*ii*). Here a single following letter (A or B, according to molecule) denotes a methylenic hydrogen, bound to the carbon sharing its first two numbers: if there are two following letters (the first of which specifies the molecule) the hydrogen belongs to the methyl carbon similarly numbered.

In compound (7a) there are no attendant methyl groups to identify readily the cage carbon atoms and, as their correct assignment was of prime importance in this experiment, we were careful to ensure the optimum procedure was followed; *i.e.* that intensity data were corrected for absorption, and a suitable weighting scheme applied to F_0, *before* inspection of the intracage distances and refined U_j parameters, all light cage atoms having been given neutral boron scattering factors. Examination of the final interatomic separations within the cage (Table 6) supports the cage carbon positions of Figure 6 (with no evidence of B/C disorder) when compared to typical B–C and B–B distances in similar molecules (Table 4).

Although pronounced differences do exist between the independent molecules A and B of (7a) in the solid state, see below, the crystallographic study therefore confirms that the *nido* to *closo* transformation (1a) ⟶ (7a) effected by pyrolytic loss of H_2 is accompanied by *carbon atom separation*. It is interesting that no species, having adjacent carbon atoms, were formed when (1a) was pyrolysed at temperatures lower than 100 °C, and that no species having non-adjacent carbon atoms were formed when (6) was pyrolysed for longer periods at 100 °C. It was only at 150 °C that (6) was converted into (7b), in which the carbon atoms are separated.

The internal stereochemistry of the $Pt(PEt_3)_2$ moieties of molecules A and B of (7a) is consistent; both adopt that described by Figure 5(*i*), in which only one angle at phosphorus [Pt(1)–P(1)–C(11), 122.4(5)° for A and

TABLE 6

Interatomic distances (Å) in the compound [*closo*-1,1-$(Et_3P)_2$-1,2,4-$PtC_2B_4H_6$] (7a)

(*a*) Molecule A			
Pt(1A)–C(2A)	2.351(13)	C(2A)–H(2A)	0.99(15)
Pt(1A)–B(3A)	2.299(15)	B(3A)–H(3A)	1.21(16)
Pt(1A)–C(4A)	2.389(11)	C(4A)–H(4A)	1.09(17)
Pt(1A)–B(5A)	2.294(14)	B(5A)–H(5A)	1.22(15)
Pt(1A)–B(6A)	2.233(16)	B(6A)–H(6A)	1.11(19)
C(2A)–B(3A)	1.552(28)	B(7A)–H(7A)	1.13(12)
C(2A)–B(7A)	1.658(19)	P(1A)–C(11A)	1.818(11)
C(2A)–B(6A)	1.540(21)	C(11A)–C(111A)	1.533(19)
B(3A)–C(4A)	1.592(21)	P(1A)–C(12A)	1.832(12)
B(3A)–B(7A)	1.816(26)	C(12A)–C(121A)	1.548(24)
C(4A)–B(5A)	1.532(26)	P(1A)–C(13A)	1.845(17)
C(4A)–B(7A)	1.650(27)	C(13A)–C(131A)	1.500(24)
B(5A)–B(6A)	1.736(26)	P(2A)–C(21A)	1.846(10)
B(5A)–B(7A)	1.769(21)	C(21A)–C(211A)	1.513(22)
B(6A)–B(7A)	1.824(24)	P(2A)–C(22A)	1.843(14)
Pt(1A)–P(1A)	2.285(3)	C(22A)–C(221A)	1.513(16)
Pt(1A)–P(2A)	2.235(2)	P(2A)–C(23A)	1.839(13)
		C(23A)–C(231A)	1.537(15)
(*b*) Molecule B			
Pt(1B)–C(2B)	2.476(11)	C(2B)–H(2B)	1.19(15)
Pt(1B)–B(3B)	2.329(13)	B(3B)–H(3B)	1.20(14)
Pt(1B)–C(4B)	2.252(13)	C(4B)–H(4B)	0.82(13)
Pt(1B)–B(5B)	2.251(19)	B(5B)–H(5B)	0.81(17)
Pt(1B)–B(6B)	2.270(15)	B(6B)–H(6B)	1.35(13)
C(2B)–B(3B)	1.537(16)	B(7B)–H(7B)	1.28(16)
C(2B)–B(7B)	1.693(26)	P(1B)–C(11B)	1.836(13)
C(2B)–B(6B)	1.557(20)	C(11B)–C(111B)	1.524(14)
B(3B)–C(4B)	1.617(22)	P(1B)–C(12B)	1.838(14)
B(3B)–B(7B)	1.834(25)	C(12B)–C(121B)	1.529(17)
C(4B)–B(5B)	1.516(17)	P(1B)–C(13B)	1.827(11)
C(4B)–B(7B)	1.728(17)	C(13B)–C(131B)	1.522(21)
B(5B)–B(6B)	1.715(21)	P(2B)–C(21B)	1.845(10)
B(5B)–B(7B)	1.781(19)	C(21B)–C(211B)	1.535(22)
B(6B)–B(7B)	1.825(19)	P(2B)–C(22B)	1.840(9)
Pt(1B)–P(1B)	2.248(2)	C(22B)–C(221B)	1.539(18)
Pt(1B)–P(2B)	2.283(3)	P(2B)–C(23B)	1.831(15)
		C(23B)–C(231B)	1.504(17)

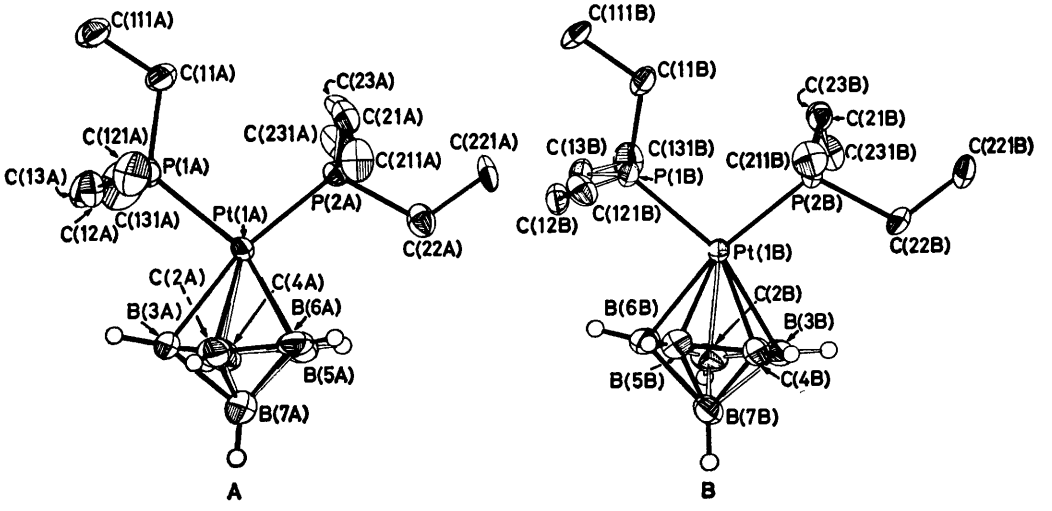

FIGURE 6 Perspective views of the crystallographically independent molecules of (7a) with only non-hydrogen atoms labelled and ethyl hydrogen atoms omitted. The projections are taken so as to show a common stereochemistry of the $Pt(PEt_3)_2$ fragments. Thermal ellipsoids as in Figure 1

120.8(3)° for B] is enlarged to relieve interligand crowding. This apart, bond lengths (Table 6) and angles (Table 7) within the phosphine ligands are unexceptional. Over both molecules ⟨P–C⟩ is 1.837(8) Å, ⟨C–C⟩ 1.525(15) Å, ⟨C–P–C⟩ 103.0(9)°, and ⟨P–C–C⟩ 114.0(19)°. One point worthy of note, however, concerns the metal–phosphorus distances. Within each molecule these are statistically different, but, in contrast * to the similar situation in (6), we here take this to represent a chemical difference since each phosphorus atom is *trans* to different (cage) environments. Furthermore, in molecule A Pt–P(1) is the longer [Δ(Pt–P) = 0.050(4) Å] whereas in B the reverse is true [Δ(Pt–P) = 0.035(4) Å]. Further comment on this is given later.

TABLE 7

Important interbond angles (°) for compound (7a)

(*i*) Molecule A	
(*a*) Deltahedral	
C(2A)–Pt(1A)–B(3A)	39.0(7)
B(3A)–Pt(1A)–C(4A)	39.6(5)
C(4A)–Pt(1A)–B(5A)	38.1(6)
B(5A)–Pt(1A)–B(6A)	45.1(7)
B(6A)–Pt(1A)–C(2A)	39.1(5)
Pt(1A)–C(2A)–B(3A)	68.7(7)
B(3A)–C(2A)–B(7A)	68.8(11)
B(7A)–C(2A)–B(6A)	69.5(10)
B(6A)–C(2A)–Pt(1A)	66.3(7)
Pt(1A)–B(3A)–C(4A)	73.2(7)
C(4A)–B(3A)–B(7A)	57.4(10)
B(7A)–B(3A)–C(2A)	58.3(10)
C(2A)–B(3A)–Pt(1A)	72.3(8)
Pt(1A)–C(4A)–B(5A)	67.6(7)
B(5A)–C(4A)–B(7A)	67.4(12)
B(7A)–C(4A)–B(3A)	68.1(11)
B(3A)–C(4A)–Pt(1A)	67.1(7)
Pt(1A)–B(5A)–B(6A)	65.6(7)
B(6A)–B(5A)–B(7A)	62.7(10)
B(7A)–B(5A)–C(4A)	59.5(11)
C(4A)–B(5A)–Pt(1A)	74.3(8)
Pt(1A)–B(6A)–C(2A)	75.6(9)
C(2A)–B(6A)–B(7A)	58.3(9)
B(7A)–B(6A)–B(5A)	59.5(9)
B(5A)–B(6A)–Pt(1A)	69.3(8)
C(2A)–B(7A)–B(3A)	52.8(10)
B(3A)–B(7A)–C(4A)	54.4(10)
C(4A)–B(7A)–B(5A)	53.1(10)
B(5A)–B(7A)–B(6A)	57.8(9)
B(6A)–B(7A)–C(2A)	52.2(8)
(*b*) Polyhedral	
P(1A)–Pt(1A)–P(2A)	101.42(10)
P(1A)–Pt(1A)–C(2A)	110.2(3)
P(1A)–Pt(1A)–B(3A)	91.2(5)
P(1A)–Pt(1A)–C(4A)	114.0(4)
P(1A)–Pt(1A)–B(5A)	151.4(5)
P(1A)–Pt(1A)–B(6A)	147.1(4)
P(2A)–Pt(1A)–C(2A)	133.9(4)
P(2A)–Pt(1A)–B(3A)	167.4(4)
P(2A)–Pt(1A)–C(4A)	131.3(4)
P(2A)–Pt(1A)–B(5A)	99.2(4)
P(2A)–Pt(1A)–B(6A)	99.3(4)
(*c*) Phosphine ligands	
Pt(1A)–P(1A)–C(11A)	122.4(5)
Pt(1A)–P(1A)–C(12A)	110.4(5)
Pt(1A)–P(1A)–C(13A)	111.9(4)
C(11A)–P(1A)–C(12A)	104.0(5)
C(11A)–P(1A)–C(13A)	103.3(7)
C(12A)–P(1A)–C(13A)	102.7(7)
P(1A)–C(11A)–C(111A)	116.3(8)
P(1A)–C(12A)–C(121A)	112.6(9)
P(1A)–C(13A)–C(131A)	114.2(12)
Pt(1A)–P(2A)–C(21A)	117.3(3)
Pt(1A)–P(2A)–C(22A)	112.3(3)
Pt(1A)–P(2A)–C(23A)	116.8(4)
C(21A)–P(2A)–C(22A)	103.2(6)
C(21A)–P(2A)–C(23A)	102.2(5)
C(22A)–P(2A)–C(23A)	103.1(5)
P(2A)–C(21A)–C(211A)	112.7(7)
P(2A)–C(22A)–C(221A)	117.2(8)
P(2A)–C(23A)–C(231A)	112.2(8)

TABLE 7 (*Continued*)

(*ii*) Molecule B	
(*a*) Deltahedral	
C(2B)–Pt(1B)–B(3B)	37.2(4)
B(3B)–Pt(1B)–C(4B)	41.3(6)
C(4B)–Pt(1B)–B(5B)	39.4(4)
B(5B)–Pt(1B)–B(6B)	44.6(6)
B(6B)–Pt(1B)–C(2B)	38.0(5)
Pt(1B)–C(2B)–B(3B)	66.2(6)
B(3B)–C(2B)–B(7B)	69.0(10)
B(7B)–C(2B)–B(6B)	68.2(10)
B(6B)–C(2B)–Pt(1B)	63.8(6)
Pt(1B)–B(3B)–C(4B)	66.8(6)
C(4B)–B(3B)–B(7B)	59.7(9)
B(7B)–B(3B)–C(2B)	59.5(9)
C(2B)–B(3B)–Pt(1B)	76.6(6)
Pt(1B)–C(4B)–B(5B)	70.3(8)
B(5B)–C(4B)–B(7B)	66.2(8)
B(7B)–C(4B)–B(3B)	66.4(9)
B(3B)–C(4B)–Pt(1B)	71.9(7)
Pt(1B)–B(5B)–B(6B)	68.3(8)
B(6B)–B(5B)–B(7B)	62.9(8)
B(7B)–B(5B)–C(4B)	62.6(8)
C(4B)–B(5B)–Pt(1B)	70.4(9)
Pt(1B)–B(6B)–C(2B)	78.2(8)
C(2B)–B(6B)–B(7B)	59.5(9)
B(7B)–B(6B)–B(5B)	60.3(8)
B(5B)–B(6B)–Pt(1B)	67.1(7)
C(2B)–B(7B)–B(3B)	51.5(8)
B(3B)–B(7B)–C(4B)	53.9(8)
C(4B)–B(7B)–B(5B)	51.2(7)
B(5B)–B(7B)–B(6B)	56.8(7)
B(6B)–B(7B)–C(2B)	52.4(8)
(*b*) Polyhedral	
P(1B)–Pt(1B)–P(2B)	100.25(10)
P(1B)–Pt(1B)–C(2B)	118.3(3)
P(1B)–Pt(1B)–B(3B)	155.4(3)
P(1B)–Pt(1B)–C(4B)	143.0(3)
P(1B)–Pt(1B)–B(5B)	104.8(3)
P(1B)–Pt(1B)–B(6B)	91.3(3)
P(2B)–Pt(1B)–C(2B)	124.5(3)
P(2B)–Pt(1B)–B(3B)	98.0(4)
P(2B)–Pt(1B)–C(4B)	107.4(3)
P(2B)–Pt(1B)–B(5B)	141.3(3)
P(2B)–Pt(1B)–B(6B)	162.4(4)
(*c*) Phosphine ligands	
Pt(1B)–P(1B)–C(11B)	120.8(3)
Pt(1B)–P(1B)–C(12B)	112.0(4)
Pt(1B)–P(1B)–C(13B)	112.9(3)
C(11B)–P(1B)–C(12B)	102.8(5)
C(11B)–P(1B)–C(13B)	104.4(6)
C(12B)–P(1B)–C(13B)	101.8(5)
P(1B)–C(11B)–C(111B)	116.4(8)
P(1B)–C(12B)–C(121B)	111.5(7)
P(1B)–C(13B)–C(131B)	114.7(7)
Pt(1B)–P(2B)–C(21B)	115.0(4)
Pt(1B)–P(2B)–C(22B)	113.3(4)
Pt(1B)–P(2B)–C(23B)	117.9(3)
C(21B)–P(2B)–C(22B)	101.6(5)
C(21B)–P(2B)–C(23B)	104.3(6)
C(22B)–P(2B)–C(23B)	102.8(5)
P(2B)–C(21B)–C(211B)	112.0(8)
P(2B)–C(22B)–C(221B)	115.0(8)
P(2B)–C(23B)–C(231B)	113.6(9)

* Interpreting the statistical difference in Pt–P lengths to only have a chemical significance in (7a) is not quite so arbitrary as it may appear, as in (6) Δ(Pt–P) is quite considerably less, 0.012(3) Å.

As Figure 6 shows, if the $Pt(PEt_3)_2$ fragments of the two molecules of (7a) are drawn so as to be superimposable, then their cages are not; rather they are related as rotational isomers. Holding the phosphine ligands fixed requires the cage of A to be rotated by more than $4\pi/5$ clockwise (when viewed from above) to attain congruence with B.*

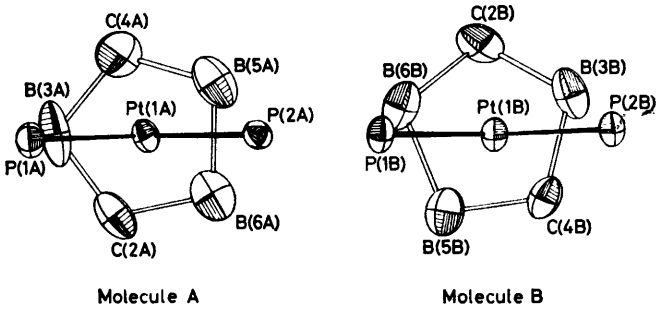

FIGURE 7 The metalla-bonded pentagonal rings of molecules A and B of (7a), seen along the bisectors of the angles P–Pt–P. Metal-to-cage links omitted for clarity

Figure 7 views the metalla-bonded rings of A and B along the bisector of each P–Pt–P angle. For molecule A one cage atom [B(3)] is situated approximately in the PtP_2 plane, whereas for B an atom [C(2)] lies in the plane perpendicular to that defined by metal and phosphorus. Thus the orientations of the PtP_2 moieties of A and B may be described [8,9] as parallel and perpendicular, respectively.

In both molecules the pentagonal rings of Figure 7 are distinctly non-planar, and in Table 8 we present the results of conformational analyses of these and other platina- or pallada-bonded five-atom faces of carbaborane ligands. For compounds (3, icosahedron, CBCBB bonded face), (4, icosahedron, CBBBB face), and (6, pentagonal bipyramid, CCBBB face) essentially envelope (C_s) conformations are adopted, in which the folding maintains the approximate cage mirror plane defined by carbon atom placement. At least partially as a result of these distortions M–C links are consistently longer than M–B [slipping of the metal fragment may also contribute, especially for (6)]. For compounds (5, icosahedron, CCBBB bonded face) and (7a, molecule A, pentagonal bipyramid, CBCBB face), the conformations approximate to skew (C_2). In each case, M–C separations are again internally longer than M–B and, indeed, both adopted skew forms occupy positions on the pseudo-rotation cycle for a five-membered ring [22] that are adjacent to the envelope conformations observed in (6) and (3) respectively.

It has previously been shown [8] that for the series of icosahedral carbametallaboranes (3), (4), and (5) distortion from planarity of the metalla-bonded face could be explained (extended Hückel molecular-orbital calculations) by a localisation of the frontier orbitals of the carbaborane ligands onto the boron atoms of the open face. These calculations invariably predict an envelope conformation for the pentagonal ligand face in which the carbon atoms dip away from metal. Perhaps because of these studies, rather than in spite of them, we and others have previously tended to assume an envelope form in attempting to quantify the distortion, even though in some cases this may not properly define the conformation. For example, in $[Cu(C_2B_9H_{11})_2]^{2-}$ (ref.

TABLE 8

Conformational analysis of metalla-bonded pentagonal rings in compounds (3), (4), (5), (6), and (7a)

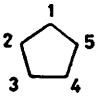

Compound	Heteroatoms	z_1 [a]	z_2	z_3	z_4	z_5	q [b]	$\langle\Delta C_s\rangle$ [c]	Nearest conformation
(3)	C(1), C(3)	−0.088 61	0.110 12	−0.083 44	0.030 65	0.031 28	0.169 88	2.3 (1.3)	Envelope, folded about 1 · · · 3
(4)	C(1)	−0.125 47	0.088 25	−0.019 41	−0.051 79	0.108 43	0.195 82	6.9 (2.3)	Envelope, folded about 2 · · · 5
(5)	C(1), C(2)	−0.003 37	−0.042 85	0.067 97	−0.066 43	0.044 68	0.113 48	15.8 (1.5)	Skew, with C_2 axis passing through 1 and midpoint of 3—4 bond
(6)	C(1), C(2)	−0.064 69	−0.048 71	0.126 18	−0.148 01	0.135 23	0.250 35	5.4 (6.0)	Envelope, folded about 3 · · · 5
(7a) Molecule A	C(1), C(3)	−0.096 13	0.100 14	−0.068 24	0.014 27	0.049 97	0.163 18	12.5 (2.0)	Skew, with C_2 axis through 4 and midpoint of 1—2 bond
(7a) Molecule B	C(1), C(3)	−0.095 29	0.074 64	−0.026 76	−0.025 00	0.072 41	0.145 72	2.0 (1.7)	Envelope, folded about 2 · · · 5

[a] z_j is the displacement (Å) of the jth atom from the least-squares plane through atoms 1—5. The metal atom lies to $+z$ in each case. [b] $q = [\Sigma(z_j)^2]^{\frac{1}{2}}$ Å. [c] $\langle\Delta C_s\rangle$, given in degrees, is the average difference between ϕ_j and the nearest ideal value (0°, 32°, 72°, 108° . . .) for a C_s conformation. Thus $\langle\Delta C_s\rangle = 0°$ represents an envelope, and $\langle\Delta C_s\rangle = 18°$ a skew conformation. $\phi_j = \{\cos^{-1}[z_j/q\sqrt{(2/5)}] - 4\pi j/5\}$. See equation (3) of J. D. Dunitz, *Tetrahedron*, 1972, **28**, 5459.

*Alternatively, molecules A and B could attain congruence by an anti-clockwise rotation of somewhat less than $2\pi/5$ if this were coupled to a synchronous rotation (π) of each PEt_3 moiety about the Pt–P vectors.

23) the true conformation is mid-way between envelope and skew [$\langle\Delta_{C_s}\rangle$ = 8.6 (4.7)°], although this structure was reported well before the m.o. calculations, whilst in [3-(Ph_3P)-3,2,1-$HgC_2B_9H_{11}$] (ref. 24) the conformation is certainly nearer to skew [$\langle\Delta_{C_s}\rangle$ = 11.4 (3.5)°]. All other slipped, 3-metalla-1,2-dicarbaboranes to have been crystallographically studied have $\langle\Delta_{C_s}\rangle$ <9°.

The barrier to $C_s \longleftrightarrow C_2$ interconversion *via* pseudo-rotation, in five-membered rings generally, is known to be extremely small and, although to our knowledge no specific data to this end are available on heteroboranes, this presumably is also the case here. Thus it is possible that crystal packing forces could readily account for such discrepancies as exist between C_s conformations predicted by theory and C_2 conformations found in some solid-state structures. In cases of skewed metalla-bonded carbaborane rings we would, however, still wish to emphasise the value of calculating the acute folding angle of the nearest (on the pseudo-rotation cycle) envelope form, so that the distortion can be quantified, at least to a first approximation, within a constant framework. Thus, for example, it is clearly of value to note that the approximate fold of (5) is substantially less than the true fold of (6).

The conformational analysis of the CBCBB ring of (7a, molecule B) reveals an envelope form which is folded across B(3) · · · B(6) such that C(2) is on the opposite side of the four-atom plane to platinum. Clearly this is at least partially responsible for the Pt(1B)–C(2B) link being >0.15 Å longer than all other metal–cage distances in this polyhedron. However, a contribution from slipping cannot be discounted but, unfortunately, neither can it be proven.

The relative orientation of metal and cage fragments in molecule B, and the magnitude (*ca.* 14.7°) and direction of the folding of its pentagonal face, bear a striking resemblance to those observed [5] in [2,2-($Bu^tNC)_2$-1-Me_3N-2,1-$PdCB_{10}H_{10}$] (4, folding angle *ca.* 16.5°) in spite of the fact that, in the latter compound, the metal atom bonds to a CB_4 polyhedral face. Accordingly, these two molecules are taken together in Table 9, in which we compare structurally similar 12- and seven-vertex carbametallaboranes. The other pairings [(3) with (7a, molecule A) and (5) with (6)] are made on the basis of molecular orientation, cage carbon atom placement, and M–B *versus* M–C distances. Other internally mutual features are the substantial slipping and folding distortions that are common to (5) and (6), and the inequalities in both magnitude and direction of Pt–P distances that are common to (3) and (7a, molecule A).

Perhaps the most significant conclusion afforded by analysis of the metal–cage atom distances in Table 9 is that, for the first two pairs of compounds, M–B lengths are maintained on passing from an icosahedron to the analogous pentagonal bipyramid. We place more emphasis on the comparison of M–B lengths since most polyhedral deformations, for example folding distortions, involve apparent movement of the carbon atoms, and we consider only the first two pairs of analogues because the greatly increased slipping distortion in (6) compared to (5) will result in anomalously short M–B bonds in the former.

TABLE 9

Comparison of metal–cage atom distances * in analogous 12- and seven-vertex carbametallaboranes

Compound	No. of polyhedral vertices	Heteroatoms	M–1	M–2	M–3	M–4	M–5	Reference
(3)	12	C(1), C(3)	*2.452(8)*	2.270(9)	*2.442(7)*	2.261(8)	2.255(9)	3
(7a) Molecule A	7	C(1), C(3)	*2.351(13)*	2.299(15)	*2.389(11)*	2.294(4)	2.233(16)	This work
(4)	12	C(1)	*2.600(6)*	2.261(6)	2.223(7)	2.259(8)	2.238(7)	5
(7a) Molecule B	7	C(1), C(3)	*2.476(11)*	2.329(13)	*2.252(13)*	2.251(19)	2.270(15)	This work
(5)	12	C(1), C(2)	*2.530(7)*	*2.613(7)*	2.277(8)	2.264(8)	2.283(8)	8
(6)	7	C(1), C(2)	*2.858(7)*	*2.851(6)*	2.257(8)	2.219(10)	2.244(8)	This work

* Italicised lengths are metal–carbon, others metal–boron. All distances in Å.

The above feature appears also to be prevalent in other comparable systems. A recent review,[25] for example, gives a typical Co–B length in an icosahedron to be *ca.* 2.07 compared with *ca.* 2.09 Å in a pentagonal bipyramid. Similarly, typical Fe–B distances in the two polyhedral types are *ca.* 2.13 and *ca.* 2.12 Å, respectively.

Thus M–B remains effectively constant in spite of the fact that, in the seven-atom systems, the equatorial boron atoms are only four-connected with respect to the polyhedron, and therefore might have been expected to have a decreased polyhedral radius. A similar phenomenon also occurs in pure B–B lengths as (Table 4) the mean $B_{ax.}$–$B_{eq.}$ distance in pentagonal bipyramids is no different to typical icosahedral distances.

Further examination of the data of Table 4 reveals that the equatorial atoms of the seven-vertex polyhedron *do* experience reduced polyhedral radii, but that this is anisotropic, occurring exclusively in the equatorial plane. Furthermore, the effect is markedly greater for links involving carbon. Thus, a typical icosahedral B–B separation of *ca.* 1.77 Å drops to *ca.* 1.71 Å (~3% reduction) in the equatorial belt of a pentagonal bipyramid, whilst B–C similarly falls from *ca.* 1.71 to *ca.* 1.57 Å

(~8%), and C–C is reduced from *ca.* 1.61 to only 1.46 Å (~9%).

Given that distances measured in the metalla-bonded ring are smaller, as one moves from the 12- to the seven-vertex system, the maintenance of M–B distances must mean that, in the latter, the metal atom is further above the co-ordinating face. This, in turn, suggests that the ligand orbitals used to bind the metal are more outpointing from the face, which is exactly the conclusion reached if one reverses a recent argument of Hoffmann and co-workers.[26] These workers considered the effect of increasing the ring size of metal–polyene fragments (with constant M–C separation) on the elevation angle of substituents terminal to the ring. As the polyene enlarges, and the metal-to-ring-plane distance falls, so the elevation angle increases. In moving from an icosahedron to a pentagonal bipyramid we *decrease* the terminal elevation angle (from 26° to 0°) and, accordingly, the metal should move further from the ring plane. The situation is sketched for one highly idealised cage m.o. in Figure 8, and from the standpoint of our present studies, this simple concept has two important consequences.

Firstly, it readily explains the increased slipping distortion in (6) compared with that in (5), whereas for the open face. Clearly, making these ligand orbitals more outpointing will cause the greatest change in the slip required in the case where three boron atoms are adjacent, the slip thereby increasing.

Secondly, it would be anticipated that a metal fragment occupying the apical vertex of a pentagonal bipyramid would enjoy a greater degree of orientational freedom, with respect to the polyhedron, than if bonded to a chemically similar icosahedral face, *i.e.* the barrier to rotation of the metal moiety about the metal–cage axis should be less in the seven-atom case.

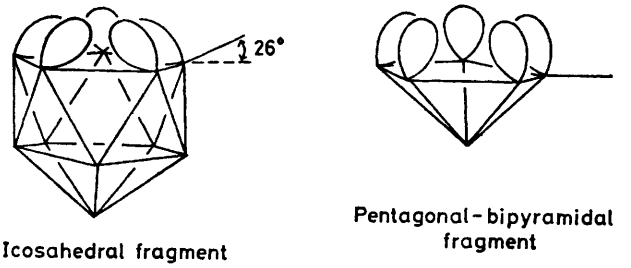

FIGURE 8 Schematic representation of the way in which a decrease in the elevation angle of terminal substituents could be expected to result in a fragment molecular orbital (localised on the open face) that is more outpointing from that face

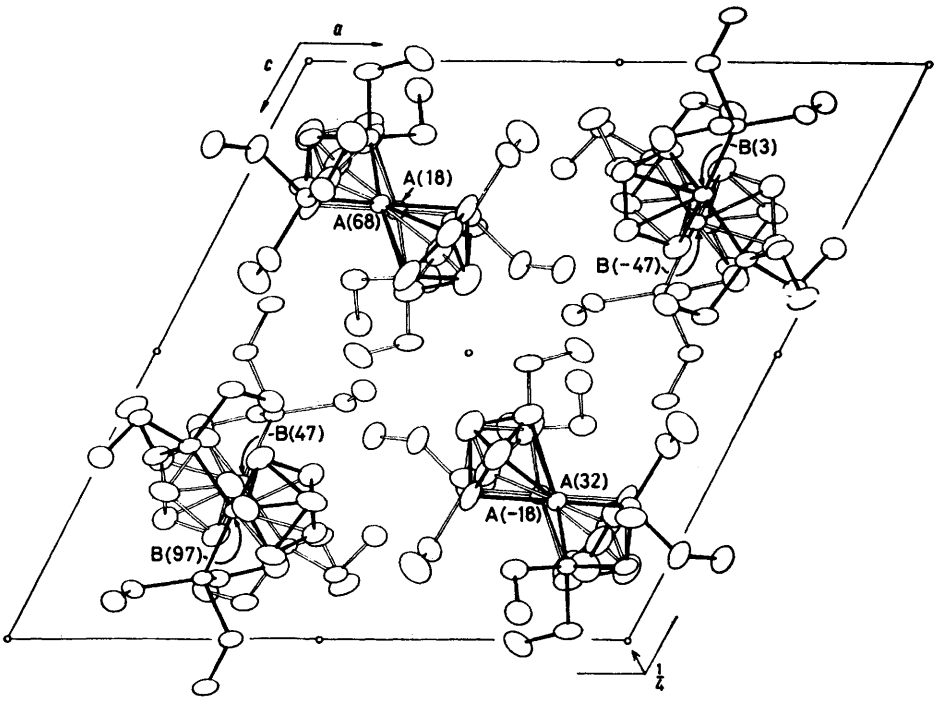

FIGURE 9 Packing diagram of (7a), as seen in *b* axis projection. The screw axis symbols and all hydrogen atoms are omitted for the sake of clarity

the other comparable pairs (Table 9) there is no such dramatic change. An extended Hückel molecular-orbital analysis[8] of the general icosahedral problem reveals that metal fragments slip because of localisation of the ligand frontier orbitals onto the boron atoms of

In agreement, the ^{31}P (^{1}H decoupled) n.m.r. spectrum of [1,1-$(Et_3P)_2$-1,2,4-$PtC_2B_4H_6$] (7a) shows evidence of dynamic behaviour explicable in terms of rotation of the $Pt(PEt_3)_2$ moiety relative to the C_2B_3 face of the cage. At 25 °C, the spectrum exhibits a broad singlet at −2.5

p.p.m. [J(PtP) 3 900 Hz], which was unaffected by ^{11}B decoupling. On cooling to −6 °C, the ^{31}P spectrum showed two singlets at −3.8 p.p.m. [J(PtP) 4 430 Hz] and −1.25 p.p.m. [J(PtP) 3 370 Hz]. In contrast the ^{31}P spectrum of [1,1-$(Et_3P)_2$-1,2,4-$PtC_2B_9H_{11}$] shows [7] two singlets at room temperature. The room temperature ^{31}P (^{11}B decoupled) spectrum of [1,1-$(Et_3P)_2$-2,4-Me_2-1,2,4-$PtC_2B_4H_4$] (7b) showed a doublet of doublets due to coupling between inequivalent ^{31}P nuclei, and only on warming to 110 °C was a singlet resonance observed, suggesting a higher barrier to rotation with the dimethyl analogue.

The crystal packing of compound (7a) is drawn in b axis projection in Figure 9. Labels such as A(−18) and B(−47) *etc.* refer to the independent molecules, giving the appropriate heights ($y \times 100$) of metal atoms above the origin plane. Table 10 lists H • • • H contacts

TABLE 10

Interligand contacts ≤2.40 Å in the crystal structure of (7a)

Atom A *	Atom B	Position B	Distance (Å)
(*a*) Intramolecular			
H(111A)	H(212A)	x, y, z	2.24
H(112A)	H(213A)	x, y, z	2.25
H(111B)	H(212B)	x, y, z	2.18
H(112B)	H(213B)	x, y, z	2.30
H(222A)	H(5A)	x, y, z	2.39
H(131BB)	H(231BB)	x, y, z	2.36
(*b*) Intermolecular			
H(131A)	H(121BC)	$x, y, z-1$	2.33
H(232A)	H(232A)	$1-x, -y, 1-z$	2.38
H(112B)	H(6A)	$\frac{1}{2}+x, \frac{1}{2}-y, \frac{1}{2}+z$	2.27
H(111BC)	H(221BB)	$\frac{1}{2}+x, \frac{1}{2}-y, \frac{1}{2}+z$	2.20
H(122A)	H(222A)	$\frac{1}{2}-x, \frac{1}{2}+y, \frac{1}{2}-z$	2.34
H(121AC)	H(5A)	$\frac{1}{2}-x, \frac{1}{2}+y, \frac{1}{2}-z$	2.37
H(221AC)	H(121BC)	$\frac{1}{2}-x, y-\frac{1}{2}, 1\frac{1}{2}-z$	2.40
H(211BC)	H(2B)	$\frac{1}{2}-x, y-\frac{1}{2}, 1\frac{1}{2}-z$	2.36
H(231AC)	H(221BC)	$\frac{1}{2}-x, y-\frac{1}{2}, \frac{1}{2}-z$	2.35

*Atom A has co-ordinates x, y, z.

≤2.40 Å. The first four intramolecular distances are associated with the $Pt(PEt_3)_2$ conformation of Figure 5(*ii*). Generally, though, the crystal structure of (7a) is free from intra- or inter-molecular crowding of any real severity.

EXPERIMENTAL

Nuclear magnetic resonance spectra were recorded on JEOL PS100 and PFT100 spectrometers (^1H, ^{11}B, ^{31}P), a Varian Associates HA-100 spectrometer (^1H, ^{11}B-decoupled), and a Brüker WP-60 spectrometer (^{13}C, ^{11}B-decoupled). The external references for 32.08 MHz ^{11}B and 40.48 MHz ^{31}P spectra were $OEt_2 \cdot BF_3$ and 85% H_3PO_4, respectively. The ^{11}B chemical shifts are to high frequency (low field) of $OEt_2 \cdot BF_3$, and the ^{31}P shifts to low frequency of H_3PO_4. All spectra were recorded in [$^2H_6$]benzene solution with ^1H decoupling unless otherwise stated. Infrared spectra were measured as Nujol mulls on a Perkin-Elmer 457 spectrophotometer. Molecular weights were measured from mass spectra recorded on a A.E.I. MS 902 spectrometer operating at 70 eV.*

All reactions were performed in a dry, oxygen-free nitrogen atmosphere or in a high-vacuum system. The complexes [*nido*-$\mu_{4,5}$-{*trans*-$(Et_3P)_2Pt(H)$}-$\mu_{5,6}$-H-2,3-$C_2B_4H_6$] (1a) and [*nido*-$\mu_{4,5}$-{*trans*-$(Et_3P)_2Pt(H)$}-$\mu_{5,6}$-H-2,3-Me_2-2,3-$C_2B_4H_4$] (1b) were prepared as reported previously.[1] The carbaborane *closo*-1,6-$C_2B_4H_6$ was a commercial sample. *closo*-1,6-Me_2-1,6-$C_2B_4H_4$ was prepared by reaction of 1,6-$Li_2C_2B_4H_4$ with MeI, and 5-Me_3N^+-2,4-$C_2B_4H_6^-$ was formed by reaction of NMe_3 with *closo*-1,6-$C_2B_4H_6$.

Pyrolytic Ring-closure of (1a).—A solution of (1a) (0.15 g, 0.3 mmol) in hexane (3 cm³) contained in a tube (100 cm³) fitted with a Westef stopcock was heated (100 °C) for 3 days, after which i.r. analysis showed that no starting material was present. The volatile material was removed *in vacuo*, and the residue extracted with hexane (20 cm³). The extract was cooled (−20 °C) to give yellow *crystals* of [*closo*-1,1-$(Et_3P)_2$-1,2,4-$PtC_2B_4H_6$] (7a) (0.05 g, 30%), m.p. 78—80 °C (Found: C, 33.7; H, 7.3%; *M*, 505. $C_{14}H_{36}B_4P_2Pt$ requires C, 33.3; H, 7.1%; *M*, 505); $\nu_{max.}$ at 2 545(sh), 2 520s, 2 500(sh), 2 485(sh), 1 415m, 1 255m, 1 158m, 1 035s, 1 000m, 888(sh), 877m, 863(sh), 768s, 725s, 715(sh), 700w, 672w, and 635m cm⁻¹. N.m.r. spectra: ^1H (^{11}B-decoupled), τ 4.87 (s, 2 H, cage C*H*), 5.25 [s(br), 1 H, apical B*H*], 6.05 [s(br), 3 H, basal B*H*], 8.37 (m, 4 H, PCH_2CH_3), and 9.14 (m, 6 H, PCH_2CH_3); ^{11}B, δ 1.8 (s, 3 B, basal B) and −7.4 p.p.m. [s, 1 B, apical B, J(BH) 164 Hz]; ^{31}P (−6 °C), δ −3.8 [s, J(PtP) 4 430 Hz], and −1.25 p.p.m. [s, J(PtP) 3 370 Hz]; ^{13}C (^{11}B decoupled), δ 9.3 (PCH_2CH_3), 21.7 (PCH_2CH_3), and 79.4 p.p.m. (cage *C*H).

Pyrolytic Ring-closure of (1b).—(*a*) Similarly, pyrolysis (100 °C, 2 h) of (1b) (0.25 g, 0.47 mmol) afforded, after crystallisation (−20 °C) from diethyl ether, yellow *crystals* of [*closo*-1,1-$(Et_3P)_2$-2,3-Me_2-1,2,3-$PtC_2B_4H_4$] (6) (0.20 g, 80%), m.p. 128—130 °C (Found: C, 37.1; H, 7.9%; *M*, 533. $C_{16}H_{40}B_4P_2Pt$ requires C, 36.0; H, 7.9%; *M*, 533); $\nu_{max.}$ at 2 540s, 2 518s, 2 465s, 2 458s, 1 418m, 1 252m, 1 138m, 1 050s, 1 040s, 1 013m, 978w, 965w, 948(sh), 939s, 890m, 780s, 728s, 685m, 645m, 600m, 520w, 440w, and 423m cm⁻¹. N.m.r. spectra: ^1H (^{11}B-decoupled), τ 1.47 [s(br), 1 H, apical BH], 5.99 [s(br), 1 H, basal BH, J(PtH) 140], 7.16 [s(br), 2 H, basal BH, J(PtH) 20], 7.74 [s, 6 H, cage Me, J(PtH) 5 Hz], 8.45 (m, 4 H, PCH_2CH_3), and 9.11 (m, 6 H, PCH_2CH_3); ^{11}B, δ 56.3 [s(br), 1 B, apical B, J(PtB) 352, J(BH) 151 Hz] and −6.32 p.p.m. [s(br), 3 B, basal B]; ^{31}P, δ −20.2 p.p.m. [J(PtP) 2 488 Hz]; ^{13}C (^{11}B decoupled), δ 149.1 (s, cage carbons), 20.5 (s, cage Me), 19.0 (m, PCH_2CH_3), and 8.7 (m, PCH_2CH_3).

(*b*) Pyrolysis of (1b) (0.3 g, 0.6 mmol) at 150 °C for 4 days afforded a brown oil, which on extraction with hexane and cooling (−20 °C) gave yellow *crystals* of [*closo*-1,1-$(Et_3P)_2$-2,4-Me_2-1,2,4-$PtC_2B_4H_4$] (7b) (0.12 g, 23%), m.p. 127—129 °C (Found; C, 36.1; H, 7.3%; *M*, 533. $C_{16}H_{40}B_4P_2Pt$ requires C, 36.0; H, 7.5%; *M*, 533); $\nu_{max.}$ at 2 530s, 2 500s, 1 410w, 1 245m, 1 150w, 1 035s, 1 000m, 949w, 900m, 766s, 760(sh), 745w, 720s, and 630m cm⁻¹. N.m.r. spectra: ^1H (^{11}B-decoupled), τ 4.96 [s(br), 1 H, apical BH], 5.98 [s(br), 3 H, basal BH], 7.40 [s, 6 H, cage Me, J(PtH) 27 Hz], 8.51 (m, 4 H, PCH_2CH_3), and 9.22 (m, 6 H, PCH_2CH_3); ^{11}B, δ 3.8 [s(br), 3 B, basal B], and −1.1 p.p.m. [s, 1 B, apical B]; ^{31}P (−80 °C), δ −5.4 and −2.5 p.p.m. [d of d, J(PtP) 4 342 and 3 419, J(PP) 19 Hz]; ^{13}C (^{11}B-decoupled), δ 96.2 (s, cage carbon), 20.8 (m, PCH_2CH_3), 19.5 (s, cage Me), and 8.2 p.p.m. (m, PCH_2CH_3).

Reaction of [$Pt_2(\mu$-cod)$(PEt_3)_4$].—(a) *With dicarba*-closo-*hexaborane* (6). An excess of *closo*-1,6-$C_2B_4H_6$ (0.6 mmol)

* Throughout this paper: 1 eV ≈ 1.60 × 10⁻¹⁹ J.

was condensed (−196 °C) into a tube (100 cm³) fitted with a Westef stopcock containing a solution of $[Pt_2(\mu\text{-cod})(PEt_3)_4]$ (0.24 g, 0.25 mmol) in hexane (10 cm³). After 24 h at 60 °C the volatile material was removed *in vacuo*. Extraction with hexane followed by cooling (−20 °C) afforded yellow crystals of (7a) (0.16 g, 62%), identical (i.r. and n.m.r.) with that described above.

(*b*) *With* 1,6-*dimethyl*-1,6-*dicarba*-closo-*hexaborane*(6). A similar reaction between *closo*-1,6-Me_2-1,6-$C_2B_4H_4$ (0.6 mmol) and $[Pt_2(\mu\text{-cod})(PEt_3)_4]$ (0.24 g, 0.25 mmol) afforded after 40 h at 60 °C and crystallisation (−20 °C) from hexane yellow crystals of (7b) (0.22 g, 82%), identical (i.r. and n.m.r.) with that described above.

(*c*) *With* 5-Me_3N-2,4-$C_2B_4H_6$. A solution of $[Pt_2(\mu\text{-cod})(PEt_3)_4]$ (0.24 g, 0.25 mmol) in tetrahydrofuran (10 cm³) was added, at room temperature, to a stirred slurry of 5-Me_3N-2,4-$C_2B_4H_6$ (0.07 g, 0.55 mmol) in tetrahydrofuran (10 cm³). After 1 h at room temperature the solvent was removed *in vacuo*. The residue was extracted with hexane, and cooled (−20 °C) to give yellow crystals of (7a) (0.1 g, 40%), identical (i.r. and n.m.r.) to that described above.

Molecular Structure Determinations.—The collection of intensity data, and the solution and refinement of the structures of (6) and (7a) followed identical lines and will therefore be described for (6) only, data in [] representing differences in respect of compound (7a).

A single, well formed crystal was selected for analysis and mounted on a thin glass fibre with a quick-setting epoxy-resin adhesive. The unit cell and space group were determined *via* oscillation and zero- and first-layer (equi-inclination) Weissenberg *X*-ray photographs taken with Cu-K_α radiation.

The crystal was then transferred to a Syntex $P2_1$ four-circle autodiffractometer equipped with a ϕ-axis low-temperature device (N_2 stream), and slowly cooled to *ca.* 215 K. When a steady state had been achieved the crystal was accurately set, and one quadrisphere of diffracted intensities collected following a well established procedure.[27] The following experimental details are relevant: 15 reflections, $15[13] < 2\theta < 25°$, were taken from a 30 min rotation photograph and accurately centred in 2θ, ω, and χ. The unit cell was chosen by inspection and the orientation matrix calculated. Data ($2.9 \leqslant 2\theta \leqslant 65.0°$ [60.0°]) were collected in two shells using graphite-monochromated Mo-K_α radiation ($\lambda_{\alpha 1} = 0.709\,26$, $\lambda_{\alpha 2} = 0.713\,54$ Å): Reflections ($0 + k + l$, $+ h + k \pm l$) were scanned (θ—2θ in 96 steps) at speeds between 0.042 5 [0.065 2] and 0.488 3° s⁻¹, the precise rate dependent upon an initial 2-s peak count in which 250.0 [150.0] and 3 000 [1 500.0] counts were used as critical thresholds. The intensities of three check reflections (3 3 6, $\bar{8}$ $\bar{1}$ 2, and 5 4 $\bar{6}$ [2 $\bar{6}$ $\bar{3}$, 7 $\bar{3}$ $\bar{2}$, and 0 0 8]) were remonitored once every 50 [100] reflections, but in neither case could we observe [28] any significant variation in their net counts as individual functions of time over the *ca.* 250 [288] h *X*-ray exposure. Of 8 322 [10 851] independent reflections measured, 7 550 [8 880] had $I \geqslant 1.0\ \sigma(I)$ and were retained for structure solution and refinement. Boundary planes were indexed and their distances from the centre of the crystal measured as accurately as possible, allowing the observed data to be corrected for absorption using the program ABSORB.[29]

Crystal Data.—Compound (6), $C_{16}H_{40}B_4P_2Pt$, M = 532.8, Monoclinic, a = 15.691(6), b = 10.118(6), c = 15.949 (6) Å, β = 115.76(3)°, U = 2 280.5(18) Å³, D_m = 1.49 at 296 K, Z = 4, D_c = 1.552 g cm⁻³ at 215 K, $F(000)$ = 1 056, μ(Mo-K_α) = 66.1 cm⁻¹, space group $P2_1/a$ (alternative setting of $P2_1/c$, C_{2h}^5, no. 14) from systematic absences.

Compound (7a), $C_{14}H_{36}B_4P_2Pt$, M = 504.7, Monoclinic, a = 16.045(7), b = 17.354(5), c = 16.918(6) Å, β = 117.11(3)°, U = 4 193(2) Å³, D_m not measured, Z = 8, D_c = 1.599 g cm⁻³ at 215 K, $F(000)$ = 1 984, μ(Mo-K_α) = 71.8 cm⁻¹, space group $P2_1/n$ (alternative setting of $P2_1/c$) from systematic absences.

Data were further corrected for Lorentz and polarisation effects, and the metal and phosphorus atomic positions deduced from a three-dimensional Patterson synthesis. With isotropic temperature factors assigned, these were refined by three cycles of full-matrix least squares and, from an accompanying electron-density difference synthesis, all non-hydrogen atoms were located. For (6) the carbon

TABLE 11

Atomic fractional co-ordinates ($\times 10^5$ Pt, P; $\times 10^4$ B, C; $\times 10^3$ H) of the refined atoms in [*closo*-1,1-$(Et_3P)_2$-2,3-Me_2-1,2,3-$PtC_2B_4H_4$] (6)

Atom	*x*	*y*	*z*
Pt(1)	2 158(1)	18 632(2)	23 389(1)
C(2)	1 007(5)	−225(7)	3 659(5)
C(3)	1 539(5)	920(7)	4 114(5)
B(4)	1 736(7)	1 842(8)	3 422(7)
B(5)	1 463(6)	932(9)	2 413(6)
B(6)	742(6)	−229(8)	2 583(5)
B(7)	1 974(6)	81(9)	3 400(6)
C(201)	830(7)	−1 348(9)	4 184(6)
C(301)	1 989(7)	1 073(11)	5 150(6)
H(4)	230(11)	258(16)	370(11)
H(5)	165(11)	114(16)	174(11)
H(6)	25(10)	−110(17)	228(10)
H(7)	268(11)	−47(15)	376(11)
P(1)	−12 474(11)	11 992(16)	12 959(11)
C(11)	−1 194(6)	595(8)	238(5)
C(111)	−957(8)	1 662(11)	−291(6)
C(12)	−2 266(5)	2 321(8)	841(5)
C(121)	−3 178(6)	1 788(9)	63(7)
C(13)	−1 682(6)	−230(8)	1 704(6)
C(131)	−1 733(7)	18(13)	2 612(7)
P(2)	379(12)	39 900(16)	27 188(11)
C(21)	−1 109(5)	4 809(7)	2 258(5)
C(211)	−1 152(6)	6 212(9)	2 579(6)
C(22)	459(6)	4 159(8)	3 974(5)
C(221)	−114(9)	3 360(11)	4 348(7)
C(23)	800(5)	5 134(8)	2 468(6)
C(231)	609(7)	5 125(12)	1 444(7)

atoms of the cage could be readily assigned since they carry terminal methyl groups, but for (7a) all ' light' cage atoms were initially treated as boron. Three more cycles of least squares were executed with platinum and phosphorus atoms allowed anisotropic thermal motion.

At this stage the variations of average $(\Delta^2 F)$ with F_o and sin θ were tested, and F_o moduli subsequently weighted such that $w = x \cdot y^{-1}$ with $x = F_o/a$ if $F_o > a$, $x = 1$ if $F_o \leqslant a$, and $y = b/\sin\theta$ if $\sin\theta < b$, $y = 1$ if $\sin\theta \geqslant b$. In this scheme a and b were assigned values of 30.0 [115.0] and 0.55 [0.30] respectively. With weights applied, the post-refinement temperature factors and internuclear distances of the cage atoms of (7a) were examined, readily revealing the true location of the carbon atoms.

For both structures, cage hydrogen positions were taken from fine-grid ΔF maps summed to a maximum $(\sin\theta)/\lambda$ of 0.5 (this technique employing only 2 273 [3 928] data) and were thereafter positionally refined (U_H* fixed at 0.04 [0.06] Å²). Hydrogen atoms of the ethyl groups were

* The isotropic temperature factor is defined as $\exp\{-8\pi^2 U(\sin^2\theta)/\lambda^2\}$.

introduced into calculated positions (assuming staggered conformations along the C–C bonds), and, although not themselves refined, were updated every fourth refinement cycle (the C–H distance was set at 1.00 Å and U_H was 0.05 [0.06] Å^2). For (6) we could not locate the six hydrogen

TABLE 12

Atomic fractional co-ordinates ($\times 10^5$ Pt, P; $\times 10^4$ B, C; $\times 10^3$ H) of refined atoms in the compound [*closo*-1,1-$(Et_3P)_2$-1,2,4-$PtC_2B_4H_6$] (7a)

Atom	*x*	*y*	*z*
(*a*) Molecule A			
Pt(1A)	26 631(3)	18 043(2)	25 554(2)
C(2A)	1 303(9)	2 563(7)	2 052(9)
B(3A)	1 639(11)	2 483(9)	1 328(11)
C(4A)	1 479(10)	1 594(8)	1 070(8)
B(5A)	1 319(11)	1 116(8)	1 749(12)
B(6A)	1 231(9)	1 790(9)	2 465(10)
B(7A)	638(11)	1 948(10)	1 267(12)
H(2A)	115(10)	307(8)	222(9)
H(3A)	176(10)	302(8)	94(9)
H(4A)	156(10)	138(8)	50(9)
H(5A)	113(10)	44(8)	178(9)
H(6A)	85(10)	172(8)	287(9)
H(7A)	−11(10)	197(8)	73(9)
P(1A)	38 935(21)	25 312(15)	26 522(18)
C(11A)	5 091(8)	2 354(7)	3 485(9)
C(111A)	5 819(9)	2 958(7)	3 553(9)
C(12A)	3 701(9)	3 551(7)	2 799(8)
C(121A)	3 674(11)	3 709(8)	3 688(10)
C(13A)	3 979(10)	2 533(8)	1 601(9)
C(131A)	4 049(13)	1 745(10)	1 270(11)
P(2A)	33 795(19)	9 931(14)	36 942(16)
C(21A)	3 940(9)	1 412(6)	4 820(6)
C(211A)	3 252(10)	1 826(7)	5 055(8)
C(22A)	2 569(9)	274(6)	3 762(7)
C(221A)	2 976(9)	−313(7)	4 503(8)
C(23A)	4 325(8)	397(6)	3 689(6)
C(231A)	3 993(10)	−91(7)	2 841(8)
(*b*) Molecule B			
Pt(1B)	24 432(3)	47 086(2)	72 608(2)
C(2B)	2 270(9)	6 124(6)	7 295(8)
B(3B)	1 487(12)	5 734(8)	6 478(8)
C(4B)	988(8)	5 148(6)	6 875(7)
B(5B)	1 525(10)	5 078(8)	7 877(9)
B(6B)	2 463(11)	5 684(8)	8 163(9)
B(7B)	1 287(11)	6 024(8)	7 420(9)
H(2B)	289(10)	655(8)	741(9)
H(3B)	118(10)	596(8)	573(9)
H(4B)	39(10)	497(8)	656(9)
H(5B)	129(10)	480(8)	810(9)
H(6B)	304(10)	590(8)	900(9)
H(7B)	74(10)	655(8)	743(9)
P(1B)	36 923(19)	41 524(14)	83 733(16)
C(11B)	4 151(8)	3 231(7)	8 207(7)
C(111B)	4 931(9)	2 862(8)	9 029(8)
C(12B)	3 493(8)	3 958(6)	9 342(6)
C(121B)	2 765(9)	3 323(6)	9 147(7)
C(13B)	4 714(8)	4 785(6)	8 849(6)
C(131B)	5 008(9)	5 115(8)	8 180(8)
P(2B)	23 892(19)	40 373(15)	60 779(15)
C(21B)	2 147(8)	2 998(6)	6 078(6)
C(211B)	1 338(9)	2 842(7)	6 303(9)
C(22B)	1 431(8)	4 343(7)	5 008(6)
C(221B)	1 431(8)	3 967(7)	4 185(7)
C(23B)	3 414(8)	4 081(6)	5 872(6)
C(231B)	3 625(9)	4 878(7)	5 663(7)

atoms of the terminal methyl groups of the cage with any real confidence, and these remain absent.

In the final stages all non-hydrogen atoms were assigned anisotropic thermal parameters and data were included only if $I \geqslant 3.0\,\sigma(I)$ (6 764 [7 165] reflections) or $3.0 > I/\sigma(I) \geqslant 1.0$ and $|F_c| \geqslant F_o$ (473 [1 110] reflections), this procedure yielding a data : variable ratio better than 32 [19] : 1. Refinement continued until no significant change occurred in any variable. R 0.067 [0.043], R' 0.079 [0.050]. A final ΔF map (all data) of 0.32 [0.35] Å resolution was featureless apart from the relatively high noise usually associated with a low $I/\sigma(I)$ threshold and some residue (*ca.* 1.5 [2.0] e Å^{-3}) around the metal atoms.

The scattering factors of ref. 30 (Pt, B), ref. 31 (P, C), and ref. 32 (H) were taken, all non-hydrogen sets being adjusted [33] for both components of anomalous dispersion. For (6), Table 11 lists the derived atomic co-ordinates (calculated H-atom positions are in Appendix A), Appendix C the thermal parameters, and Appendix D the structure factors. Equivalent data for (7a) are contained in Table 12 (Appendix B for H atoms), and Appendices E and F respectively. Although initial solution and refinement was accomplished with the Syntex XTL system,[34] final refinement employed programs of the ' *X*-Ray '72 ' package, implemented on the CDC 7600 computer of the University of London Computer Centre. Diagrams were constructed using Johnson's ORTEP-II.[35]

We thank the U.S. Air Force Office of Scientific Research for support, and NATO for a grant. A. J. W. thanks Dr. H.-B. Bürgi and Professor J. D. Dunitz (E. T. H., Zurich) for discussions concerning the conformational analysis.

[9/1623 *Received*, 12*th October*, 1979]

REFERENCES

[1] Part 10, G. K. Barker, M. Green, F. G. A. Stone, A. J. Welch, T. P. Onak, and G. Siwapanyoyos, *J.C.S. Dalton*, 1979, 1687.
[2] M. Green, J. L. Spencer, F. G. A. Stone, and A. J. Welch, *J.C.S. Dalton*, 1975, 179.
[3] A. J. Welch, *J.C.S. Dalton*, 1975, 1473.
[4] G. K. Barker, M. Green, J. L. Spencer, F. G. A. Stone, B. F. Taylor, and A. J. Welch, *J.C.S. Chem. Comm.*, 1975, 804.
[5] W. E. Carroll, M. Green, F. G. A. Stone, and A. J. Welch, *J.C.S. Dalton*, 1975, 2263.
[6] (*a*) A. J. Welch, *J.C.S. Dalton*, 1975, 2270; (*b*) *ibid.*, 1976, 225; (*c*) *ibid.*, 1977, 962.
[7] M. Green, J. L. Spencer, and F. G. A. Stone, *J.C.S. Dalton*, 1979, 1679.
[8] D. M. P. Mingos, M. I. Forsyth, and A. J. Welch, *J.C.S. Dalton*, 1978, 1316.
[9] D. M. P. Mingos, *J.C.S. Dalton*, 1977, 602.
[10] R. N. Grimes, W. J. Rademaker, M. L. Denniston, R. F. Bryan, and P. T. Greene, *J. Amer. Chem. Soc.*, 1972, **94**, 1865.
[11] D. C. Beer, V. R. Miller, L. G. Sneddon, R. N. Grimes, M. Mathew, and G. J. Palenik, *J. Amer. Chem. Soc.*, 1973, **95**, 3046; G. J. Palenik, personal communication to A. J. W.
[12] W. T. Robinson and R. N. Grimes, *Inorg. Chem.*, 1975, **14**, 3056.
[13] W. M. Maxwell, E. Sinn, and R. N. Grimes, *J. Amer. Chem. Soc.*, 1976, **98**, 3490.
[14] R. Weiss and R. F. Bryan, *Acta Cryst.*, 1977, **B33**, 589.
[15] J. R. Pipal and R. N. Grimes, *Inorg. Chem.*, 1978, **17**, 10.
[16] G. K. Barker, M. Green, T. P. Onak, F. G. A. Stone, C. B. Ungermann, and A. J. Welch, *J.C.S. Chem. Comm.*, 1978, 169.
[17] R. J. D. Gee and H. M. Powell, *J. Chem. Soc.* (*A*), 1971, 1956.
[18] G. W. Bushnell, K. R. Dixon, and M. A. Khan, *Canad. J. Chem.*, 1974, **52**, 1367.
[19] M. Green, J. A. K. Howard, J. L. Spencer, and F. G. A. Stone, *J.C.S. Dalton*, 1975, 2274.
[20] P. B. Hitchcock, B. Jacobson, and A. Pidcock, *J. Organometallic Chem.*, 1977, **136**, 397.
[21] A. J. Welch, unpublished work.
[22] See, for example, Figure 3 of C. Altona and M. Sunaralingam, *J. Amer. Chem. Soc.*, 1972, **94**, 8205.
[23] R. M. Wing, *J. Amer. Chem. Soc.*, 1967, **89**, 5599.
[24] H. M. Colquhoun, T. J. Greenhough, and M. G. H. Wallbridge, *J.C.S. Dalton*, 1979, 619.
[25] D. M. P. Mingos and A. J. Welch, unpublished work.

[26] M. Elian, M. M. L. Chen, D. M. P. Mingos, and R. Hoffmann, *Inorg. Chem.*, 1976, **15**, 1148.
[27] A. G. Modinos and P. Woodward, *J.C.S. Dalton*, 1974, 2065.
[28] A. G. Modinos, 'DRSYN,' a Fortran program for data analysis.
[29] Technical Report TR–192 of the Computer Science Centre, University of Maryland, June 1972.
[30] D. T. Cromer and J. T. Waber, *Acta Cryst.*, 1965, **18**, 104.
[31] D. T. Cromer and J. B. Mann, *Acta Cryst.*, 1968, **A24**, 321.
[32] R. F. Stewart, E. R. Davidson, and W. T. Simpson, *J. Chem. Phys.*, 1965, **42**, 3175.
[33] 'International Tables for *X*-Ray Crystallography,' Kynoch Press, Birmingham, 1974, vol. 4.
[34] Copyright 1973, Syntex Analytical Instruments, Cupertino, California.
[35] C. K. Johnson, 'ORTEP-II,' ORNL–5138, Oak Ridge National Laboratory, Tennessee, March 1976.